Modal analysis of a grand piano soundboard at successive manufacturing stages

Roberto Corradi, Stefano Miccoli, Giacomo Squicciarini[1]

Politecnico di Milano, Department of Mechanical Engineering, Via G. La Masa 1, 20156 Milano, Italy

Paolo Fazioli

Fazioli Pianoforti, Via Ronche 47, 33077 Sacile, Italy

Abstract

This paper deals with the development and validation of a Finite Element numerical model of a grand piano soundboard, studied at successive manufacturing stages. Experimental modal analysis results are presented and compared with corresponding numerical simulations, that include modelling of the manufacturing process. The advantage of the approach illustrated in the paper lies in the possibility of using it to better understand the influence of specific technical solutions on the piano behaviour, thus providing effective support to the instrument designers.

Keywords: experimental modal analysis, numerical modeling, FEM, piano soundboard, piano making

1. Introduction

In a piano the soundboard has the role of converting string vibration into sound. Strings and soundboard are connected through bridges and the soundboard itself is stiffened by a set of ribs running perpendicular to the main direction of wood grain. Despite is apparent simplicity, a grand piano soundboard is a complex structure, whose elaborate manufacturing process introduces subtle changes in its shape and even stress state. From the origin of the scientific studies on pianos [1] it was found that even the most slight modification of the soundboard geometry can have a perceptible effect on the tone quality. Specifically it is believed that all the following soundboard characteristics need to be considered and opportunely designed: the

[1]Currently Institute of Sound and Vibration Research, University of Southampton.

This manuscript has been published in Applied Acoustics on April 26, 2017.
The final version of record is available at
https://doi.org/10.1016/j.apacoust.2017.04.010

board variable thickness ("diaphragmed" soundboard), the ribs section and spacing, the material properties, the residual curvature after ribs gluing ("crown"), the static deflection due to the vertical string loads ("downbearing") with the consequent residual stresses, the bridge position, and the way the soundboard is glued onto the rim. At the purpose of correlating these characteristics with the final tone quality, piano manufacturers are looking for reliable methodologies capable of predicting the acoustic behaviour of their instruments under design modifications, thus limiting the need of building prototypes.

The literature on piano acoustics is vast and covers aspects from hammer–string contact to sound propagation. We will focus our attention on those studies specifically devoted at testing and modelling the soundboard or that include the soundboard as an important aspect of the research. Several examples exist in the literature dealing with vibration testing performed at the purpose of validating and updating numerical models or simply aimed at characterising the vibrational and acoustic behaviour of the structure. Suzuki [2] presented a modal analysis of a grand piano soundboard below 200 Hz and acoustic and vibration measurements up to 5.4 kHz to estimate the soundboard radiated power and radiation resistance. Measurements were performed on a soundboard with rim but without strings and cast-iron frame. In this condition Suzuki found that the acoustic power radiated while exciting the soundboard at single points is strongly affected by vibration modes up to 500 Hz. Kindel and Wang [3] described one of the first *Finite Element* (FE) models of piano soundboard: by using a small number of shell and beam elements the first few modes of the soundboard were obtained. The piano structure was modelled via beam elements and the vibration modes up to 130 Hz were compared with experiments. Kindel and Wang also discussed the importance of modelling the rim of the piano to obtain the correct series of modes at low frequencies. Conklin [4] presented various examples of modal testing and mechanical impedance measurements. Different aspects of soundboard design were touched in this review paper; of particular interest are the description of role of the bridge, which reduces the point mobility at the strings connection points (if compared to the bridgeless board), the effects of string tension and the presence of ribs making the soundboard behave as a periodic structure with periodic attenuations.

In the 1990s Giordano *et al.* developed a complete model of the piano [5–9]: the main idea was that of using the Newton's law to describe the energy flow in the piano in the time domain. The soundboard's behaviour was modelled by solving, via finite differences, the equation of motion of a thin orthotropic plate. More recently another complete computational model of the piano was presented by Chabassier *et al.* [10]. In this case the soundboard was modelled as a Reissner-Mindlin plate with space variable mechanical properties so that variable thickness and variable ribs spacing could be accounted for.

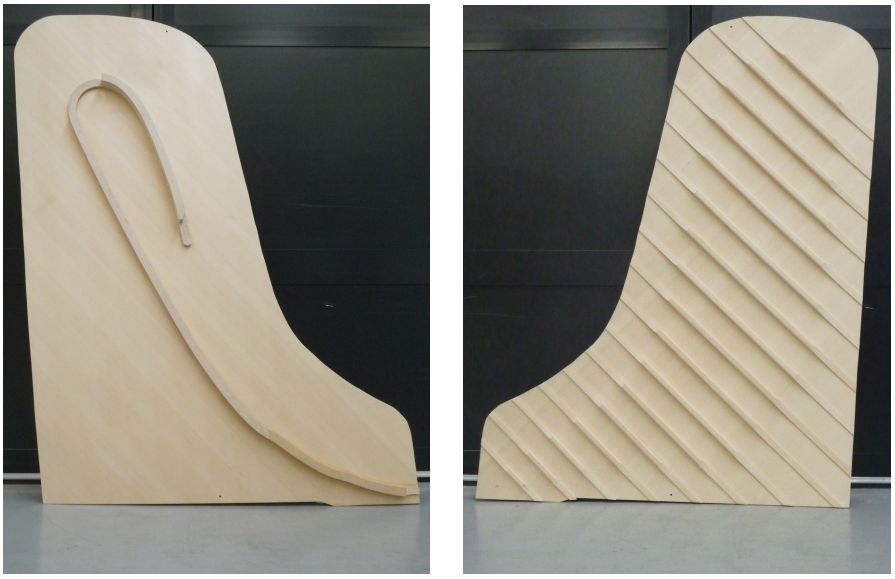

Figure 1: Upper and lower view of a Fazioli F278 soundboard.

Berthaut *et al.* [11] described an experimental modal analysis campaign performed on a grand piano soundboard in free-edge boundary condition along with a corresponding FE model. Numerical results were compared with experiments and a good correspondence was found up to nearly 250 Hz. Moore and Zietlow [12] developed a method of electronic speckle pattern interferometry in order to measure the soundboard deflection shapes. The comparison presented between their measurements and a simplified FE model of the structure showed that the vertical force exerted by the strings on the soundboard has a non-negligible effect on the natural frequencies of the lowest modes, while it can be neglected when working in the mid/high frequency range. Mamou-Mani *et al.* [13] presented a FE model of the soundboard to study the effect of the crown and downbearing. It was observed that nonlinear solution is required when the effect of these two parameters have to be taken into account. Results were presented in the frequency range corresponding to individual mode resonances, i. e. up to 450 Hz. These outcomes were later experimentally confirmed [14]. In a recent study Chaigne *et al.* [15] focused on the influence of the ribs spacing and showed that above 1 kHz there is a localisation effect which is very sensitive to small changes in the spacing itself.

This paper illustrates the main results of a research project aimed at developing a vibroacoustic numerical model of the soundboard, to be used as a support for instrument design. Attention is focused on the experimental modal analysis carried

out on the soundboard of a Fazioli F278 grand piano (Fig. 1) and on the FE model that has been developed in parallel. The main idea behind the authors' research is that accurate FE modelling is important for developing a predictive vibro-acoustic simulation tool. Moreover a detailed structural model, that includes also the manufacturing process, is valuable if it has to be used as an effective design aid. A step-by-step procedure has been adopted to validate the FE model. This approach is based on the idea of performing modal analysis tests at four significant stages of the soundboard manufacturing process: free soundboard before bridge gluing, free soundboard after bridge gluing, soundboard glued on the rim (before stringing and tuning), and the finished instrument, complete with iron frame and tuned strings. This step-by-step approach has been adopted for two main reasons. The first is that it allows investigating on how the single phases of the piano manufacturing process influence the vibration properties of the soundboard. The second and most important reason is related to the objective of simplifying the development of the soundboard FE model: by performing a step-by-step validation, the model is expected to reach better reliability and accuracy. To this end, the development of the FE model proceeds in parallel to the experimental tests, by reproducing the soundboard configuration at the same four manufacturing stages. The FE model takes into account the tapering as well as the curvature of the board. Peculiar to the presented approach is that the soundboard curvature is not assumed *a priori* but it is obtained by explicitly simulating the manufacturing process. As a side effect, the presence of the induced self-stresses is also considered.

Some details on the manufacturing process are given in sect. 2, while modal testing is described in sect. 3. The FE model and the parameter updating algorithm are illustrated in sect. 4 and 5. Finally, experimental and numerical results are compared in sect. 6.

2. Manufacturing stages

Four main phases of the soundboard manufacturing process are singled out to be simulated by FE analysis and experimentally investigated. At the end of each manufacturing phase the soundboard is at a "production stage" numbered from STAGE 1 to STAGE 4. The very first production step defines a STAGE 0, corresponding to the starting configuration of the analysis.

2.1. Preliminary preparation, STAGE 0.

The construction of the F278 soundboard starts by edge gluing quarter-sawn small planks of Norway spruce; the resulting panel is then shaped, planed, seasoned, and finally tooled by a *Computer Numerically Controlled* (CNC) milling machine to achieve a carefully controlled variable thickness. This process is called

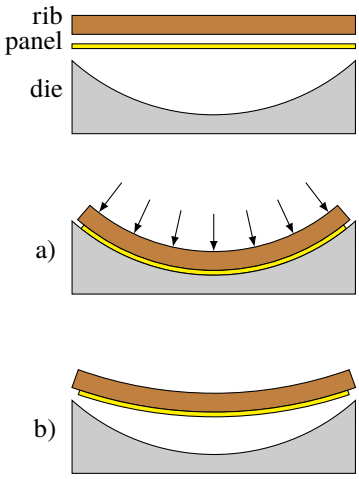

Figure 2: Compression crowning by gluing straight ribs to a flat panel in a curved die. (a) pressure is applied on the ribs while liquid adhesive allows rib–panel slip; (b) after adhesive curing, pressure is removed and a residual curvature is obtained due to rib–panel stick. The curvature of the die is exaggerated for clarity.

"diaphragming" in the piano industry, a term which refers to the thinning of the soundboard near the edges. The use of quarter-sawn planks guarantees that the wood anatomical directions are almost constant across the panel: longitudinal and radial (L, R) in the plane of the soundboard, tangential (T) normal to the surface. In Fig. 1 the L direction can be easily recognised from the wood grain.

2.2. Gluing of the ribs and crowning, STAGE 1.

In the finished piano the soundboard is subjected to a considerable load due to the tension and the angle of the strings across the bridges. This load is normal to the soundboard surface and has a resultant of about 3 kN. To withstand this load and to avoid an excessive deformation, the soundboard has to be stiffened by a system of ribs on the surface opposite to the bridges. Spruce has a very low stiffness in the cross grain directions (see Tab. 1): therefore the ribs have to run perpendicular to the spruce grain. The ribs themselves are made of spruce, with grain parallel to their length.

In order to better control the deflection of the soundboard under the load of the tensioned strings, the ribs are assembled to the panel by means of a peculiar procedure that causes an initial reverse deflection, called "crown" in the piano industry. There are several methods for obtaining the desired crown, the most simple one consisting in using curved ribs, i. e. "rib crowning". For the soundboard under

investigation a different procedure is adopted, based on initially straight ribs. The ribs are glued to the panel in a special press with a curved die. When pressure is applied, the adhesive is still liquid and both ribs and panel are free to assume the shape of the die; as it is clear from Fig. 2 this is accompanied by a relative sliding between panel and ribs. After adhesive curing any further slip is prevented; therefore, when pressure is removed elastic springback occurs but ribs and panel cannot return to the initial straight and flat configuration. As a consequence the soundboard shows a residual curvature and a residual self-stress field. Owing to the low bending stiffness of the panel in the cross grain direction, its internal stresses are mainly compressive, while bending dominates in the ribs. For this reason the method is called *compression* crowning. (Other crowning methods introduce mainly bending in the panel, see [16].)

The initial geometry of panel, ribs and die is known, along with all the material properties, but the final "crowned" shape and the self-stress field are unknown. Both these two features can affect the vibroacoustic properties of the soundboard, and hence the tonal quality of the finished piano. While the final shape can be measured, internal stresses are hard to assess experimentally. In this paper we present a method to estimate these by a FE simulation of the gluing process.

2.3. Gluing of the bridges and planing down of the ribs, STAGE 2.

The bridges are glued to the opposite side of the panel, with a process that closely resembles the ribs assembly, but the curvature of the die is chosen to be not so different from the curvature of the soundboard at STAGE 1. Therefore one has to expect only a slight modification of both the curvature and self stress state. Finally the ribs are planed down at the ends, to obtain their final shape: during this process self-stresses are partially released, but the curvature of the soundboard increases, owing to the reduced the stiffness of the ribs. Fig. 1 shows the soundboard at STAGE 2.

Again, while the soundboard shape at STAGE 2 can be measured, the self-stress state is unknown: therefore both bridge gluing and ribs planing have been included into the FE simulation.

2.4. Final assembly, STAGE 3 *and* STAGE 4.

From the manufacturing point of view, at STAGE 2 the construction of the soundboard itself is concluded and the remaining steps involve assembly into the complete piano. However during assembly new constraints are imposed and loads are applied to the soundboard, causing vibrational properties to change. For the purpose of the present investigation two further stages are defined.

At STAGE 3 the soundboard is assembled in the piano case by gluing its edge on the internal rim. The internal rim itself is fitted to the curved shape of the

soundboard, in order to prevent additional stresses due to the new constraints. The case is much stiffer than the soundboard and in first approximation can be assumed rigid.[2] STAGE 4 corresponds to the finished piano. The strings exert a downward force which causes a deflection of the soundboard called "downbearing" and the crown is consequently reduced. This phenomenon changes the vibration properties of the soundboard (see [13]).

3. Experimental modal analysis

3.1. Test procedure

The experimental tests were carried out at each one of the manufacturing stages mentioned before. In particular, at the Fazioli factory in Sacile (Italy), the soundboard at STAGE 1 (before bridge gluing, see Fig. 3(a) and STAGE 2 (after bridge gluing) was tested by suspending it on a steel cable so as to reproduce a free-edge boundary condition. The length of the cable was chosen so as to set the system first natural frequency below 2 Hz. This choice allowed the sound board rigid motion and its flexible vibration modes to be decoupled. The soundboard was instrumented with 10 piezoelectric uniaxial accelerometers (sensitivity $10\,\mathrm{mV\,s^2\,m^{-1}}$, range $10\,000\,\mathrm{m\,s^{-2}}$, bandwidth 10 kHz, mass 2 g). The tests were performed using two different impact hammers: first a large impact hammer (160 g mass) with a soft tip allowed investigating the low/mid frequency range (up to 1 kHz), then the impact tests were repeated using a small hammer (5 g mass) with an harder tip, to excite higher frequencies. By means of the latter device it was possible to introduce enough energy into the system so as to measure the soundboard *Frequency Response Function* (FRF) up to approximately 5 kHz. However, based on the purpose of this paper, attention is focused on a frequency range limited to 1 kHz. The tests were repeated for two excitation points and six different accelerometer positioning, so as to cover a regular measurement grid with 60 nodes in total, equally spaced on a 200 mm × 200 mm square mesh.

Analogous tests were performed for the STAGE 3 (see Fig. 3(b)), at the Department of Mechanical Engineering of Politecnico di Milano. Due to the higher weight of the structure under test, the piano case was resting on three supports located under the rim, so as to weakly affect the soundboard vibration behaviour. During STAGE 3, in addition to the accelerometers positioned on the 200 mm × 200 mm measurement grid, an interferometric laser velocimeter (Polytec PSV-400,

[2] A more detailed analysis shows that its flexibility is expected to have some influence on the soundboard natural frequencies, especially for low order modes [3].

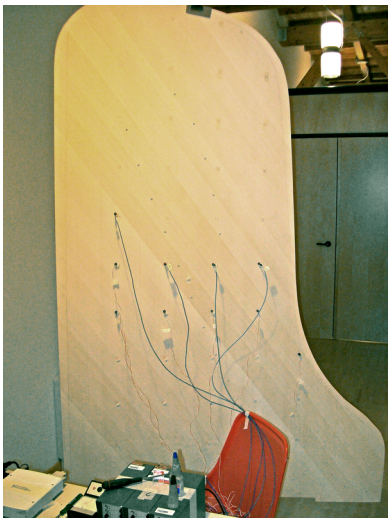

(a) STAGE 1: free soundboard before bridge gluing.

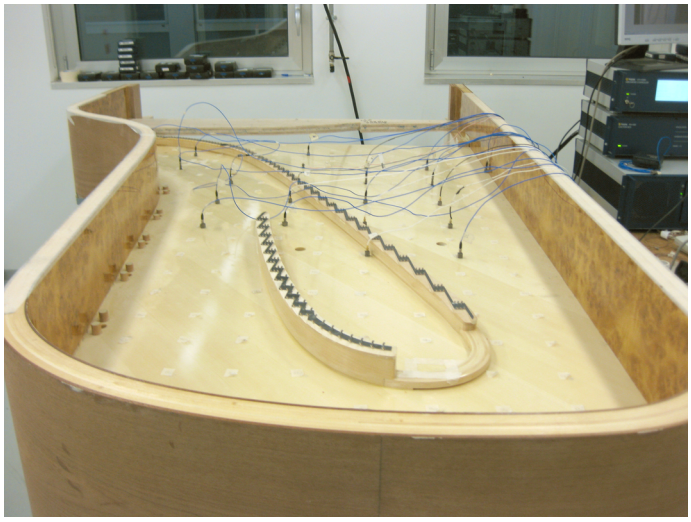

(b) STAGE 3: soundboard assembled on the piano structure.

Figure 3: Experimental modal analysis at different manufacturing stages.

with adjustable sensitivity and measurement range) was used to scan a 100 mm × 100 mm grid.

The H_1 estimator ([17]) was adopted to derive the soundboard FRF's from the collected experimental data:

$$H_{jk}(\omega) = \frac{G_{jk}(\omega)}{G_{kk}(\omega)}, \tag{1}$$

where G_{kk} is the autospectral density function of the input force f_k, G_{jk} the cross-spectral density function between the input force f_k and the output vibration x_j, and H_{jk} the H_1 estimate of the FRF between f_k and x_j. The coherence function γ^2_{jk} between f_k and x_j was calculated too, which provides a measure for the quality of the FRF data:

$$\gamma^2_{jk}(\omega) = \frac{|G_{jk}(\omega)|^2}{G_{jj}(\omega)\, G_{kk}(\omega)}. \tag{2}$$

The calculation of G_{jj}, G_{kk}, and G_{jk} was carried out according to the procedure indicated by Bendat and Piersol [18], which consists in computing the *Fast Fourier Transform* (FFT) for each block of sampled data (corresponding to one single impact test), then the corresponding raw autospectral/cross-spectral density functions for each *j*–*k* node pair, and in finally averaging over the data blocks corresponding to the ten impact test repetitions, for fixed j and k.

Two examples of mobility FRF's and associated coherence functions are reported in Figs. 4(a) and 4(b) (solid line), which refers to the measurements carried out at STAGE 1 and STAGE 3, for the same pair of excitation and measurement points (both located close to the bridge, in correspondence with the positions where the bridge itself is crossed by the $A\sharp_4$ and $D\sharp_3$ strings respectively). In this case, the soundboard was excited by the small hammer and the output vibration was measured by means of a piezo-accelerometer. However, during the tests, it was checked that the FRF's obtained by different combinations of the excitation and measurement equipment were in very good agreement, so as to be confident with the reliability and accuracy of the measurement process.

3.2. Natural modes identification

The identification procedure used for the estimation of modal parameters from experimental FRF's consists in a two-step approach.

First, the *Least Squares Complex Exponential* (LSCE) algorithm [19–21] is applied to estimate the system poles and the corresponding natural frequencies and damping ratios. This is a time-domain algorithm which requires as input the *Impulse Response Function*s (IRF's) for all the considered *j*–*k* pairs. The IRF's is obtained by computing the inverse FFT of FRF data. Typically the LSCE estimator

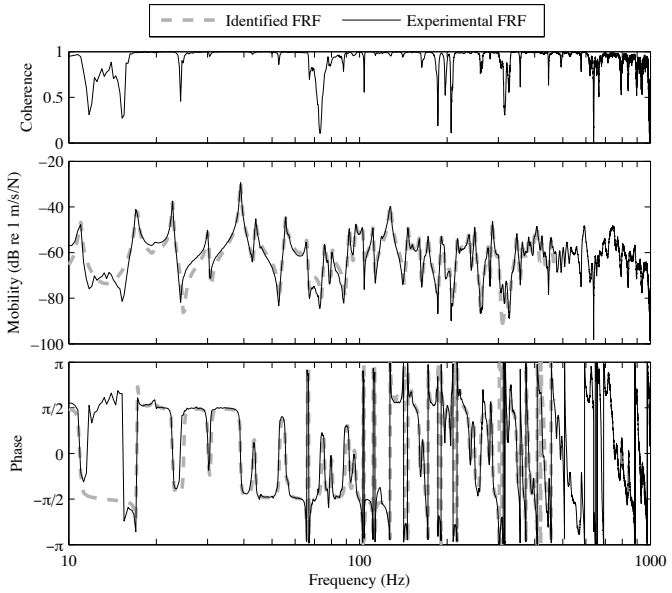

(a) STAGE 1: free soundboard before bridge gluing.

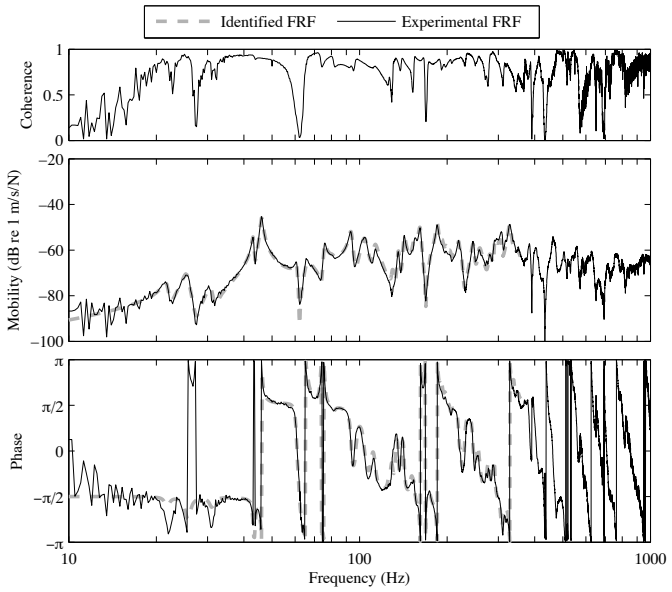

(b) STAGE 3: soundboard assembled on the piano structure.

Figure 4: Comparison between experimental and identified FRF.

is applied assuming different model order: therefore a stabilisation chart is obtained [19, 21], which allows selecting the system physical poles considering their stability for increasing model order.

The second step consists in the classical FRF-based curve-fitting method [17]: according to the idea of modal superposition, the measured FRF's are fitted with an analytic model consisting of a series of second order systems. Least squares minimisation operates in a user-defined frequency band which includes a certain number of vibration modes: a limited variation of their natural frequencies and damping ratios with respect to the previous LSCE estimates is allowed. To reach suitable curve-fit, high and low frequency residuals are added to the resonant modes [17], so as to account for the contribution of the modes not included in the selected frequency band. The adopted frequency-domain algorithm allows simultaneous processing of the whole FRF experimental data set. The final output are the modal parameters (i. e. natural frequencies, damping ratios and mode shapes) of the vibration modes included in the frequency band of interest.

The reliability of the overall identification process can be finally verified by visually checking the accuracy of the FRF fitting: looking at Figs. 4(a) and 4(b), it can be concluded that the identified FRF (dashed line) reproduces the experimental one in a fully satisfactory way. By following this procedure these sets of vibration modes were identified: 52 modes up to 450 Hz for the soundboard at STAGE 1, 39 modes up to 386 Hz for soundboard at STAGE 2, 34 modes up to 348 Hz for soundboard at STAGE 3. The identified damping ratios vary from 0.4 % to 1.0 % for the first two stages, from 0.8 % to 4.0 % for the third stage.

The three construction stages correspond to three different structures, in terms of configuration and especially constraints and damping. This results in three different values of the transition frequency between the low-frequency range, which is characterised by individual modal resonances, and the mid/high-frequency range, which shows coupled multi-mode response. Identification algorithms for modal parameter estimation can be efficiently applied only in the low-frequency range, were the overlap factor [22] is limited, i. e. modes are clearly spaced and the system shows limited damping. In Figs. 4(a) and 4(b) the identified FRF's, for STAGE 1 and STAGE 3, respectively, are plotted only up to the transition frequency mentioned above.

4. Finite Element model

As outlined in sect. 2, the construction of a soundboard is a complex procedure: the geometry and the self-stress state attained at each stage is the outcome of the preceding manufacturing process. Since geometry and self-stress state are not known *a priori*, at each manufacturing stage a "standalone" FE model cannot

be used to predict the actual natural frequencies, but has to be tuned against experimental data [11]. To overcome this difficulty in the present paper a different FE modelling strategy was pursued: instead of creating a sequence of different "stage" models, each with its own tuning problems, a direct simulation of the whole manufacturing process is presented. By doing so the "model state" and its modal properties at each stage can be included in the model without *ad hoc* assumptions. Model tuning is performed at STAGE 1, and only to the purpose of updating material elastic constants, as outlined in sect. 5, (see also Tab. 1.) At the subsequent stages (STAGE 2 and following) no further tuning is necessary.

In this section the modelling of the manufacturing process is described, while natural frequencies extraction and material parameters update is postponed to section 5.

The manufacturing process has been modelled by means of a fully nonlinear FE model, i. e. taking into account finite strain, arbitrary displacement and stress-stiffening effects. During the whole manufacturing process dynamic effects are negligible, so that a quasi-static calculation is appropriate. Material behaviour can be considered linear (see eq. (A.1) and Tab. 1) due to the low loads involved. Creep effects have been neglected.

All FE analyses were carried out using the finite element program Abaqus/Standard v. 6.10. This is a general-purpose nonlinear FE code that is organised around the concept of an "analysis problem history" defined in terms of "steps". Each step is associated with an "analysis procedure" that defines the type of analysis to be performed, [23]. This approach maps nicely to the present problem in which the "manufacturing history" of the soundboard has to be simulated. Since the problem is quasi-static, the Abaqus "static stress analysis" (keyword `*STATIC`) procedure has been used throughout the analysis. In order to account for the geometric nonlinearities linked to a large-displacement formulation, the `*STEP, NLGEOM` keyword was specified.

In order to break up the manufacturing process into analysis steps, a careful analysis of both the physical process and the FE numerical convergence properties has to be performed. (In a nonlinear FE simulation "large steps" in which many different processes and transformation occur tend to have grater convergence problems than "small steps" in which the state change is limited.) For the study presented in the present paper, a rather fine grained approach was adopted: the manufacturing is split into many smaller steps, in order to have a better control on the numerical convergence, at the cost of a more complex model setup. Within this approach, a manufacturing STAGE is simply the state of the FE model at the end of a given key analysis step.

4.1. FE *model at* STAGE 0

The soundboard at STAGE 0 is the starting point of the present analysis i. e. the reference (initial) state of the FE model.

At STAGE 0 the soundboard is modelled as a stress-free, variable thickness, flat solid plate made of an homogeneous material. In reality the soundboard is obtained by gluing together smaller wooden planks, but the inhomogeneities intrinsic to wood and those due to the not perfect alignment of the anatomical directions between different planks are not relevant at the macroscopic scale. Moreover the adhesive has a negligible thickness with respect to the planks in-plane dimensions but still it guarantees a very strong bonding, so that no stress/strain discontinuities have to be expected along the adhesion planes. Finally no internal stresses are present after the first fabrication steps that lead to STAGE 0.

Wood is a complex natural material, but to the purposes of the present analysis it can be modelled as an homogeneous orthotropic elastic material, with the anatomical directions (L, R, T) aligned to the elasticity principal axes (1, 2, 3) [24]. According to equation (A.1), an orthotropic material is characterised by the nine elastic parameters E_1, E_2, E_3, ν_{12}, ν_{13}, ν_{23}, G_{12}, G_{13}, and G_{23}; moreover the mass density ρ has to be considered for modal analysis. It is easy to understand that determining these nine moduli plus mass density is a hard task, since they can be defined only in a statistical sense: wood from different logs has different properties, owing to the varying micro and macro climatic conditions that affect tree growth. Even specimens from the same log, but taken from different annual rings exhibit different material properties. Finally the same specimen changes its properties according to moisture content, seasoning, rate of loading.

Instead of trying a direct measurement of these ten material properties, an initial educated guess was made about their value, based on the data available from the literature (mainly from [24]); the chosen values are listed in Tab. 1, under the column "initial". As it will be made clear in the sequel (sect. 5) these initial values were updated by comparing the predicted natural frequencies to the measured ones, so that their precise initial estimate is not critical.

For an appropriate choice of the soundboard FE's, one has to consider that the gluing process between the lower/upper face of the soundboard with the ribs/bridges has to be simulated. Moreover, due to diaphragming, the thickness is not constant across the board. For these reasons a solid model is convenient, but still, due to the small thickness, a thin shell model is adequate. This is why Abaqus "Continuum Shell" elements `SC8R` [23] were chosen for modelling the soundboard. About 6000 elements where used, with an average in-plane edge $\approx$ 20 mm. The element size and type where chosen so as to generate a mesh compatible with the maximum frequency of interest, i. e. 4 kHz. The board 3D geometry was obtained directly from

Table 1: Wood mechanical properties. Anatomical directions (L, R, T) are aligned to orthotropy principal directions (1, 2, 3).

		panel *picea abies*		ribs *picea sitchensis*		bridges *acer*
		initial	updtd.	initial	updtd.	estimated
E_1	(GPa)	12.8	14.6	13.4	12.7	12.6
E_2	(GPa)	0.625	0.686	1.04	1.04	1.66
E_3	(GPa)	0.397	0.436	0.397	0.478	0.819
ν_{12}		0.36		0.37		0.42
ν_{13}		0.45		0.47		0.48
ν_{23}		0.48		0.43		0.77
G_{12}	(GPa)	0.617	0.677	0.864	0.998	1.40
G_{13}	(GPa)	0.587	0.644	0.830	0.959	0.793
G_{23}	(GPa)	0.053	0.058	0.045	0.042	0.500
ρ	($\mathrm{kg\,m^{-3}}$)	437.	452.	505.	489.	630.

the same CAD models used for generating the working profiles of the diaphragming CNC milling machine.

4.2. FE *model at* STAGE 1 *and* STAGE 2

STAGE 1 and STAGE 2 essentially involve two types of procedures:

- ribs and bridge gluing and
- ribs planing down.

4.2.1. Ribs and bridge gluing

The main idea is to handle the gluing process by simulating a contact problem without an explicit model of the adhesive layer. When the adhesive is still liquid one has frictionless unilateral "hard" contact between the surfaces to be glued; this means that no penetration (overclosure) is allowed, relative sliding (slip) of arbitrary entity is permitted as well as surface separation (contact opening). After adhesive curing the contact conditions are changed to "tie", i. e. no separation and no sliding is permitted. The rationale for this model is that the adhesive layer is very thin and therefore the contribution to stiffness and mass of the adhesive itself can be neglected. On the other hand the bond is very strong, and in normal working conditions one does not expect any adhesive failure.

Ribs gluing is performed in a curved die, see Fig. 2, which has been modelled as a rigid surface; the ribs themselves have been modelled with hexahedral, reduced

integration, linear FE's (Abaqus C3D8R). On average the ribs where meshed with 3×3 elements on the cross section, with an edge of about 7 to 10 mm. The material has been modelled as homogeneous, linear elastic, orthotropic: material properties are given in Tab. 1 as Sitka spruce.

The FE simulation of the actual gluing of the ribs involved many analysis steps. In the first step, condition (a) of Fig. 2, has been simulated as a frictionless unilateral contact problem, where the ribs are subjected to a pressure load so as to keep the board/ribs system in contact with the die, Fig. 5(a). Afterwards the board-to-ribs contact condition was transformed into "tie", and the applied pressure removed: the ensuing equilibrium state is possible only with an elastic springback, but the soundboard cannot recover the original stress-free state, due to adhesion, see Fig. 2(b): the crowning at the end of the gluing process is clearly visible in Fig. 5(b).

It is worth noting that, in order to correctly represent the physical process of compression crowning, several type of nonlinearities have been taken into account: unilateral contact, finite-sliding, finite displacements, and stress stiffening. Moreover, during the spring-back analysis, the soundboard is not constrained, and numerical instabilities may arise. In order to achieve convergence, the loading and unloading of the soundboard had to be divided into many small load steps. Pressure was applied and removed on one rib at a time, to avoid to have to solve for too severe nonlinearities in a single attempt/load increment.

An analogous procedure was applied for simulating the gluing of the bridge, which is assumed for simplicity as made of maple (see Tab. 1). The ensuing analysis steps are not detailed here for brevity.

4.2.2. Ribs planing down

The planing down procedure was simulated simply by element removal. This technique is very common in damage evolution modelling: when the material corresponding to a given finite element is "damaged" it does not contribute anymore to the structural behaviour, and it can be simply cancelled form the model. Similarly, when a portion of a rib is taken away by the planing machine, the corresponding elements are removed from the model. This reduces the stiffness of the soundboard, resulting in an increase of the crowning.

4.3. Final stages 3 and 4

At STAGE 3 the gluing of the soundboard to the piano case is simulated. But now a simpler approach can be adopted. In fact the rim is "fitted" to the soundboard edge curved shape, so that no changes in the soundboard configuration and self-stress state are to be expected. For the sake of simplicity the piano case was assumed to be so stiff that after gluing it can be modelled simply by ideally clamped

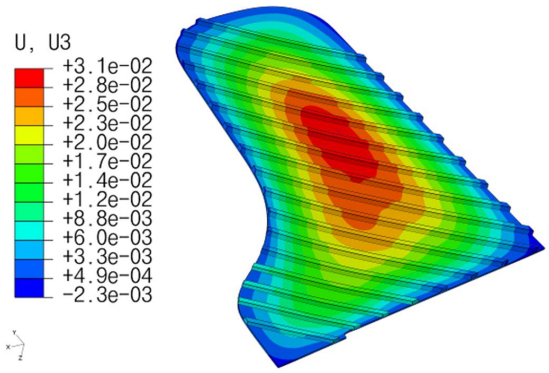

(a) No adhesion, pressure applied, board and ribs in die.

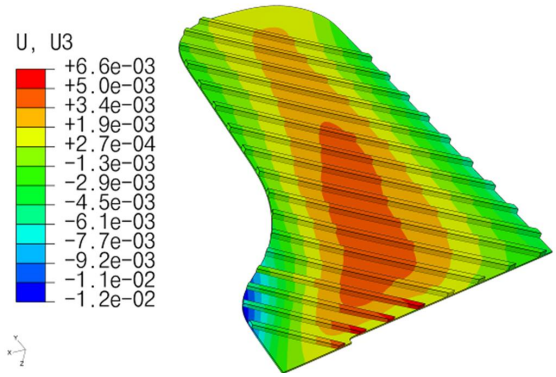

(b) After glue adhesion, pressure removed, and elastic springback out of the die.

Figure 5: Simulated ribs gluing procedure. Displacement field in the direction normal to the board, units are (m).

boundary conditions. As already noted, this assumption will introduce some error on the estimate of the soundboard natural frequencies, especially in the low frequency range. Better results could be obtained by coupling the soundboard model to a FE model of the case itself, but this approach will not be pursed in this paper.

Finally for STAGE 4, the load of the strings is added as a set of concentrated loads on the bridges, one for each note. Since stress-stiffening effects are accounted for, this will result in a change of the soundboard eigenfrequencies, as already noted in [13].

5. Natural frequency extraction and material properties updating

For a nonlinear FE method the equilibrium equations are not expressed in terms of a stiffness matrix but directly from the principle of virtual works, as a balance between nodal equivalent external forces and nodal equivalent internal forces. In order to define natural frequencies and modes a linearisation of the equilibrium equations is necessary, in order to define a *tangent stiffness matrix*, [25]. More precisely, given a sequence of nonlinear steps $\{\mathcal{S}_i\}$, linearisation at the end of each step allows to compute the *tangent* stiffness matrix $\mathbf{K}_{\mathrm{T}}^{\mathcal{S}_i}$; when a finite displacement formulation is used, like in the present case, the mass matrix has to be computed with reference to the current reference configuration, giving raise to a $\mathbf{M}^{\mathcal{S}_i}$ that changes with $\mathcal{S}_i$. Eigenfrequencies and eigenmodes at step $\mathcal{S}_i$ are therefore defined from the generalised eigenproblem

$$(-\omega_{\mathcal{S}_i}^2 \mathbf{M}^{\mathcal{S}_i} + \mathbf{K}_{\mathrm{T}}^{\mathcal{S}_i})\, \mathbf{u}_{\mathcal{S}_i} = \mathbf{0}. \tag{3}$$

From the above equation it is evident that the computed eigenfrequencies and eigenmodes change with $\mathcal{S}_i$. Note that no damping is introduced into the FE model, so that real eigenvalues/eigenvectors are computed. However since large-displacement formulation is used (Abaqus `*STEP, NLGEOM` keyword) the computed eigenfrequencies will take into account the actual curved geometry (crown and downbearing) and internal stress state.

To summarise, analogously to the experimental modal analysis results, where one has different natural frequencies at different manufacturing stages, the FE computed natural frequencies will change as the analysis history proceeds: by identifying the key analysis steps, it is possible to predict the natural frequencies numerically at different manufacturing stages.

The outcome of the eigenfrequency analysis strongly depends on the material properties, the initial estimates of which are given in Tab. 1. Given all the uncertainties in determining wood properties by means of direct measurement, the material parameters were tuned so as to best fit the computed eigenmodes on the

corresponding experimental data at STAGE 1. Indeed, starting from a tentative value of the material parameters, a set of natural frequencies and normal modes can be obtained. These numerical values are compared to the experimental ones, and the elastic material properties are identified by applying an error minimisation technique, as outlined below.

5.1. Modal assurance criterion and experimental to numerical mode pairing

The first task to be solved is to pair numerical mode shapes and experimental ones, so as to compare the corresponding natural frequencies. Both the experimental modes and the numerical ones are known at discrete locations: accelerometer positions on the measurement grid and FE nodes, respectively. FE nodes are far more numerous than accelerometers: special care was given in order to position a FE node at each position of the measurement grid, in order to allow for direct comparison. Thanks to this, both numerical and experimental modes can be characterised by a vector of displacement components $\mathbf{u}$, where the FE vector is just extracted from the eigenvector pertaining to the whole model.

In order to pair numerical and experimental modes the *modal assurance criterion* (MAC) was adopted [26]. In general, for complex valued vectors $\mathbf{u}$ and $\mathbf{v}$, the MAC value is defined as

$$\mathrm{MAC}(\mathbf{u}, \mathbf{v}) = \frac{|\mathbf{u}^{\mathrm{H}}\mathbf{v}|^2}{\|\mathbf{u}\|^2\|\mathbf{v}\|^2} \tag{4}$$

where $\mathbf{u}^{\mathrm{H}}$ is the conjugate transpose of $\mathbf{u}$, $|z|^2 = \bar{z}z$ is the squared modulus of the complex number z, and $\|\mathbf{u}\|^2 = \mathbf{u}^{\mathrm{H}}\mathbf{u}$ is the squared ℓ^2-norm of $\mathbf{u}$. It can be shown that $0 \leq \mathrm{MAC}(\mathbf{u}, \mathbf{v}) \leq 1$, where $\mathrm{MAC} = 1$ is attained when vectors $\mathbf{u}$ and $\mathbf{v}$ are identical up to a complex modal scaling factor, while $\mathrm{MAC} = 0$ denotes completely uncorrelated modal vectors.

The general MAC criterion can also be used in the present case, where the eigenmodes are real valued: in (3) no damping was introduced, while the identified experimental modes are assumed to be real-valued under the hypothesis of lightly damped system. Denoting by $(f_{\mathrm{x}}^{(r)}, \mathbf{u}_{\mathrm{x}}^{(r)})$, $r = 1 \dots P$ the set of experimentally identified natural frequencies and modes and by $(f_{\mathrm{n}}^{(s)}, \mathbf{u}_{\mathrm{n}}^{(s)})$, $s = 1 \dots Q$ the numerical ones, a MAC-matrix $\mathbf{M}$ with elements

$$M_{rs} = \mathrm{MAC}(\mathbf{u}_{\mathrm{x}}^{(r)}, \mathbf{u}_{\mathrm{n}}^{(s)}) \tag{5}$$

can be defined. Two modes $(f_{\mathrm{x}}^{(p)}, \mathbf{u}_{\mathrm{x}}^{(q)})$ and $(f_{\mathrm{n}}^{(q)}, \mathbf{u}_{\mathrm{n}}^{(q)})$ are paired if $M_{pq} > m_{\mathrm{t}}$, where m_{t} is a suitably defined threshold. If N_{pair} is the number of paired modes, this procedure defines a mapping (p_i, q_i), $i = 1 \dots N_{\mathrm{pair}}$, between the paired experimental and numerical mode indexes p, q.

5.2. Material parameters updating at STAGE 1

At STAGE 1 the soundboard is made of Norway spruce (board) and Sitka spruce (ribs), the elastic properties of which are described by 10 parameters each, see Tab. 1. First of all a *Design Sensitivity Analysis* (DSA) was performed on the first 40 modes of the soundboard, calculating the change in natural frequency caused by small changes in each elastic constant. This procedure showed that only a limited number of elastic properties needed to be taken into account for model updating. The most important were found to be E_1 of both Norway and Sitka spruce. DSA demonstrated also that E_2 of Norway spruce has an effect on the natural frequency smaller than E_1 of Sitka spruce as the ribs tend to dominate the stiffness in this direction. Changes in G_{13} of Sitka spruce affect natural frequencies only below the tenth mode. The other moduli and Poisson ratios have negligible impact and were not included in the updating procedure.

As a consequence of DSA and considering uncertainties in the density and overall stiffness of the wood, the following six parameters were selected for independent updating:

- a common scaling factor for all the elastic moduli of both woods;
- a scaling factor for all the elastic moduli of Sitka Spruce alone;
- E_1 of Sitka spruce;
- E_1 of Norway spruce;
- ratio E_1/G_{13} for Sitka spruce;
- density of Sitka spruce (density of Norway spruce is consequently updated to match the soundboard mass measured at STAGE 1 during modal testing).

The purpose of the material parameters updating is to obtain a better match between the numerical simulation and the experimental data. If one has N_{pair} paired modes (r_i, s_i), $i = 1 \dots N_{\text{pair}}$, the objective is to minimise

$$g = \sum_{i=1}^{N_{\text{pair}}} \alpha^2 \left[1 - \frac{f_{\text{n}}^{(s_i)}}{f_{\text{x}}^{(r_i)}}\right]^2 + \beta^2 \Big[1 - M_{r_i s_i}\Big]^2 \tag{6}$$

i. e. to have better natural frequency and mode shape matching. The evaluation of g requires the solution of a multi-step nonlinear FE analysis, and obviously has a highly nonlinear dependence on the material parameters under investigation.

A solution to the above defined minimisation problem was pursued by coupling the MATLAB non linear least square solver `lsqnonlin` and Abaqus itself.

No claim is made about having computed a *true* optimal solution in this way. In fact special care was dedicated in finding physically admissible values for the material parameters: therefore somewhat arbitrary but realistic bounds were imposed on the material parameters in the least squares solving process. After numerous experiments, the updated parameters presented in Tab. 1 were considered acceptable for the purpose of the present investigation. A representation of the MAC matrix after material updating for STAGE 1 to stage3 is given in Fig. 6.

Material updating by matching numerical and experimental data was performed only at STAGE 1: the idea is that the material parameters should be determined once, for the simplest structure, and then kept constant throughout the subsequent stages.

6. Numerical–experimental comparison

Figs. 7 to 9 show the comparison between numerical and experimental modes, in terms of natural frequency, MAC value, and visual representation of the mode shapes. The comparison is repeated for stages 1 to 3 and for the first 6 modes of each stage. In Tab. 2 the comparison is extended to the first 20 experimental modes. All the numerical results correspond to the updated material parameters, obtained from the procedure described in the previous section.

Given that in the experiments of stages 1 and 2 the soundboard was suspended on a steel cable, the tested condition exactly corresponds to the free-edge boundary condition assumed in the FE simulations. Therefore a one-to-one correspondence between numerical and experimental modes is found, with the only exception of a limited number of experimental modes that do not have a FE counterpart.

In the case of STAGE 3 the situation is different. While the tested structure is the soundboard assembled in the piano case (resting on three supports located under the rim), the FE one is the soundboard alone, clamped all along its edge. The latter modelling choice corresponds to assuming the rim to be infinitely rigid. On the contrary, experimental modal analysis at STAGE 3 revealed that the soundboard–rim structural coupling results in vibration modes duplications, i. e. the same mode computed through the clamped-edge FE model may correspond to more than one experimental mode (with very similar shape but different natural frequency). This circumstance is evidenced through the way numerical and experimental modes of STAGE 3 are associated in Tab. 2. Note that the clamped-edge assumption of the FE model leads to a systematic overestimation of the natural frequencies. Going back to figure 9, for the sake of simplicity, in case of mode duplications, only one experimental mode (the one with the higher natural frequency) is shown.

The results reported in Tab. 2 refer to the low frequency range, i. e. the range where experimental modal analysis can be successfully performed and single vibration modes identified. Actually, it is well known that the FRF of a plate-like

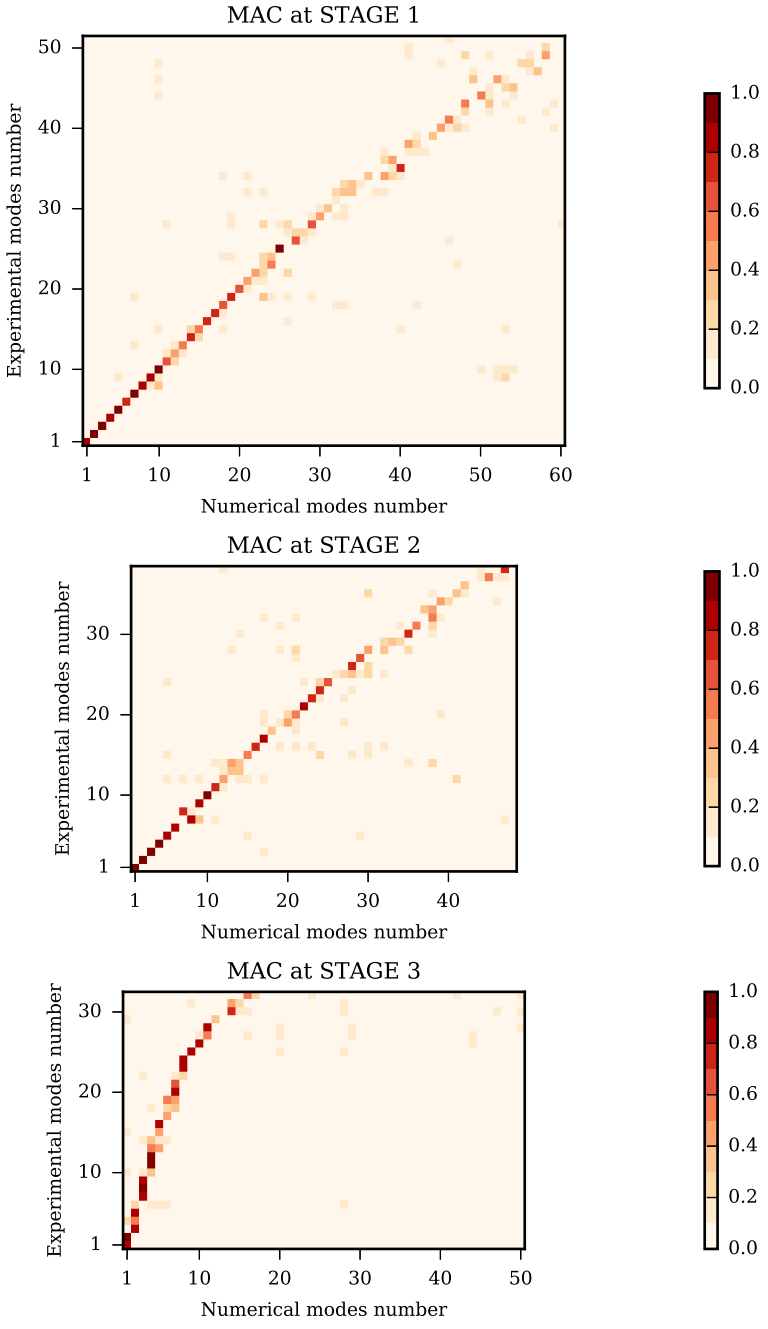

Figure 6: Colour scale representation of the numerical to experimental MAC matrix, after material parameter updating.

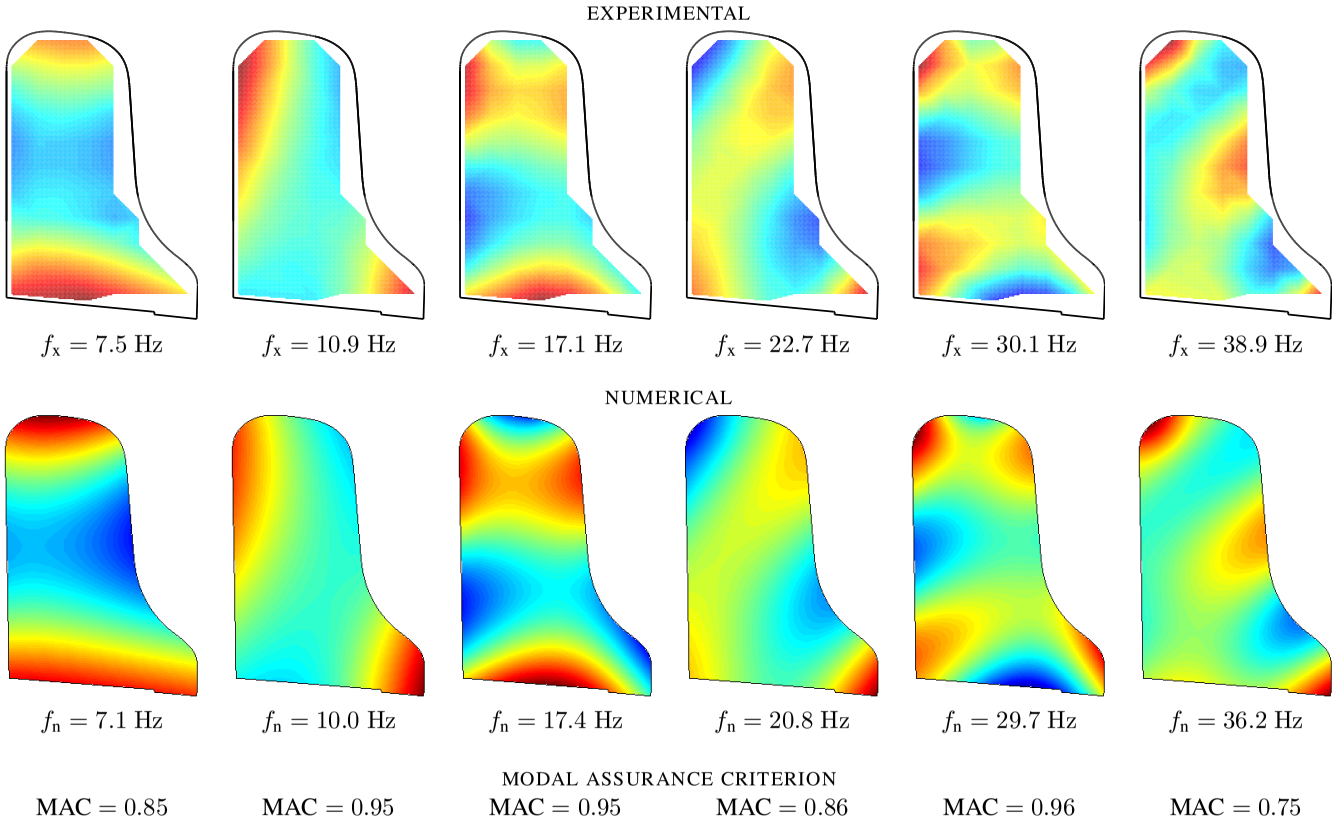

Figure 7: STAGE 1: experimental vs. numerical vibration modes.

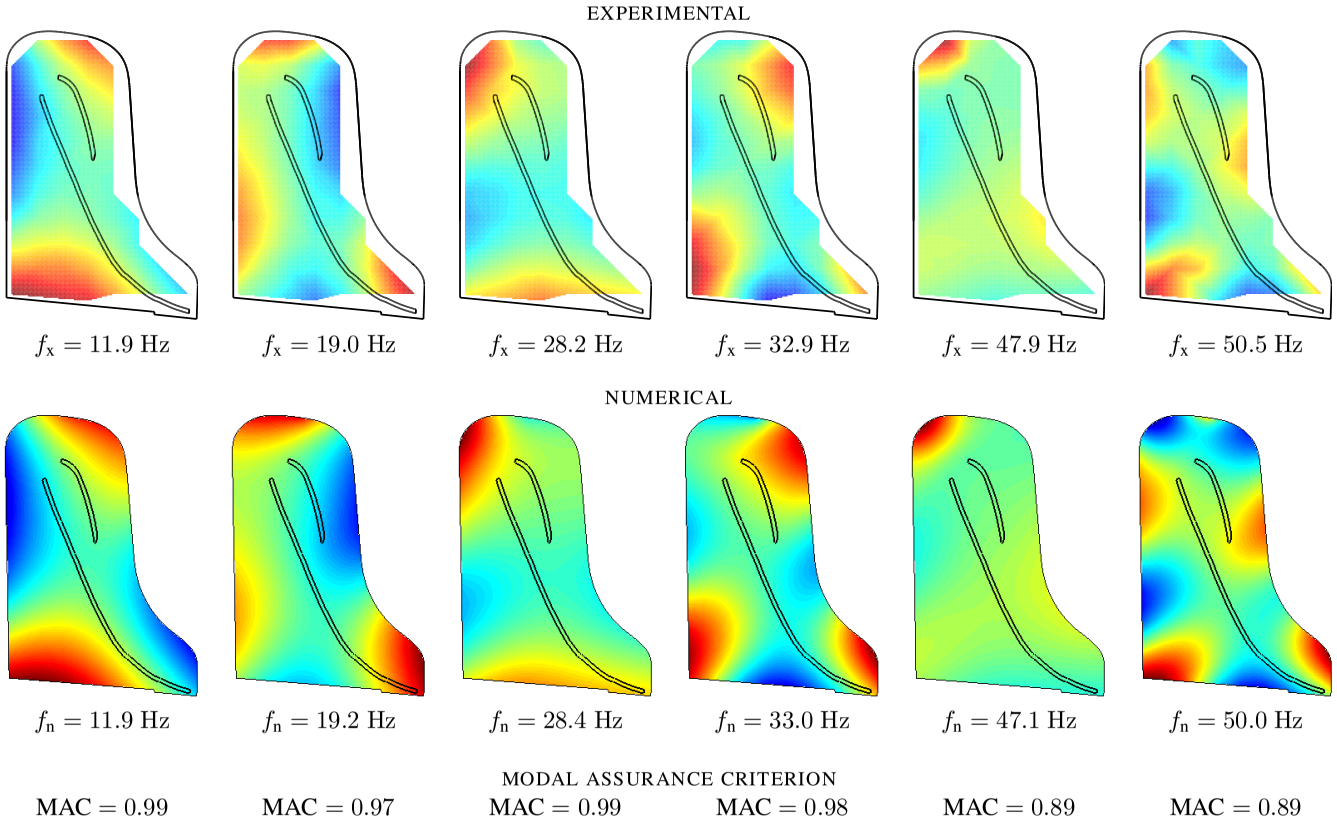

Figure 8: STAGE 2: experimental vs. numerical vibration modes.

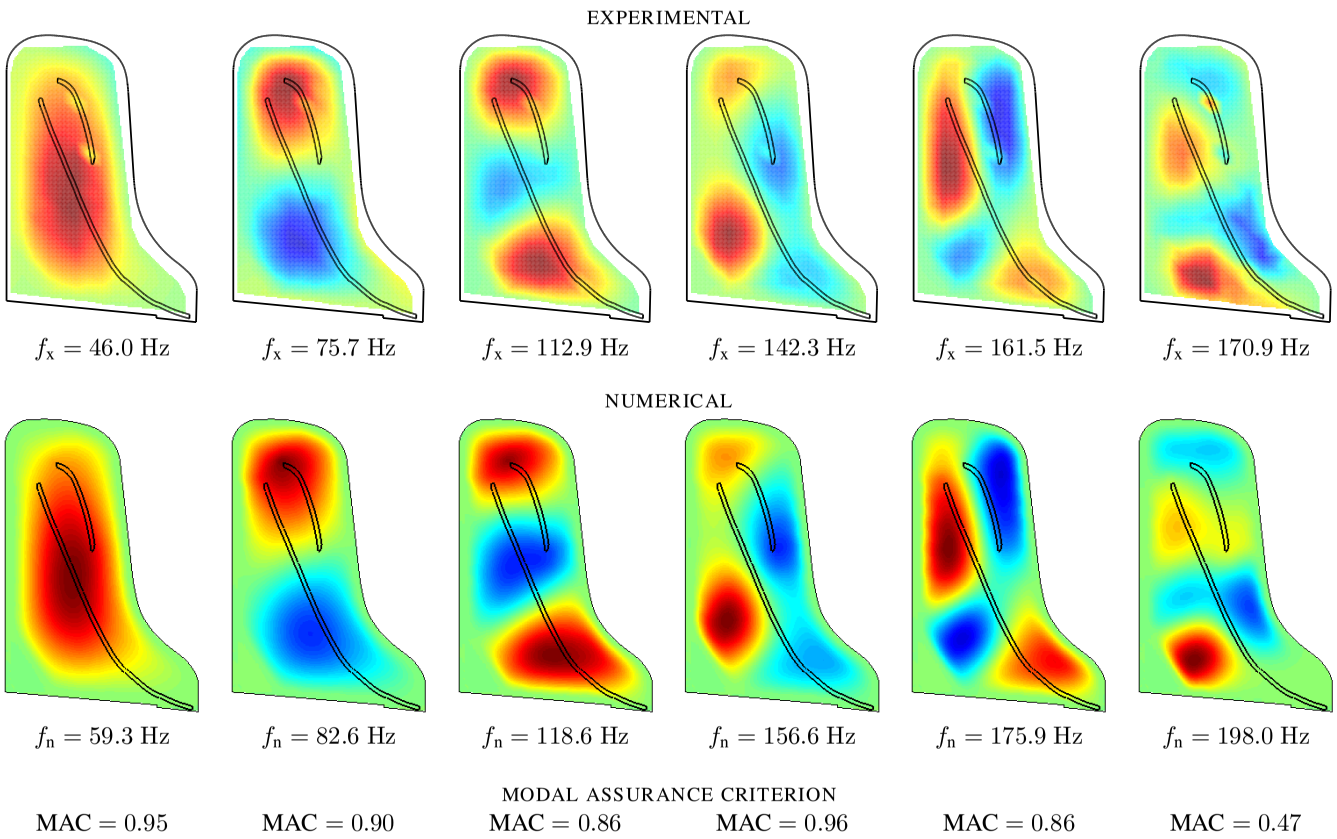

Figure 9: STAGE 3: experimental vs. numerical vibration modes.

Table 2: Experimental vs. numerical vibration modes.

STAGE 1			STAGE 2			STAGE 3		
nat. freq. of the experimental modes (Hz)	MAC	nat. freq. of the numerical modes (Hz)	nat. freq. of the experimental modes (Hz)	MAC	nat. freq. of the numerical modes (Hz)	nat. freq. of the experimental modes (Hz)	MAC	nat. freq. of the numerical modes (Hz)
7.5	0.85	7.1	11.9	0.99	11.9	43.1	0.88	59.3
10.9	0.95	10.0	19.0	0.97	19.2	46.0	0.95	
17.1	0.95	17.4	28.2	0.99	28.4	60.8	0.81	
22.7	0.86	20.8	32.9	0.98	33.0	65.7	0.58	82.5
30.1	0.96	29.7	47.9	0.89	47.1	75.7	0.90	
38.9	0.75	36.2	50.5	0.89	50.0	81.3		
43.8	0.95	43.6	61.1	0.87	65.5	93.5	0.86	
55.7	0.85	53.1	63.3	0.75	64.7	103.9	0.95	118.6
56.7	0.87	57.2	70.9	0.80	74.5	112.9	0.86	
65.9	0.94	65.4	77.7	0.91	80.4	126.3		
74.3	0.64	74.1	85.6	0.78	89.5	135.9	0.92	
75.8			89.9			142.3	0.96	156.6
80.5	0.58	81.2	100.7			151.5	0.50	
92.1	0.71	92.6	105.8	0.49	105.9	153.6		
96.9	0.58	97.7	111.4	0.54	115.7	157.1		
102.4	0.74	104.5	125.9	0.72	128.1	161.5	0.86	175.9
111.2	0.73	112.7	131.4	0.85	133.7	170.9	0.47	198.0
119.1	0.63	115.2	139.1			174.8		
127.5	0.71	128.7	153.3	0.45	157.7	185.0		
134.8	0.69	136.3	167.1	0.54	170.6	191.2	0.81	204.8

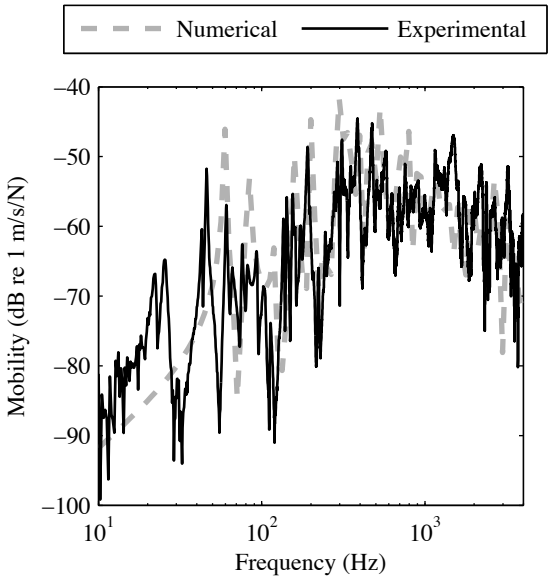

Figure 10: STAGE 3: experimental vs. numerical FRF.

structure is dominated by individual resonances in the low-frequency range, while at higher frequency the increasing modal density makes it impossible to separate the different modes. In the specific case analysed in this paper, the transition frequency between these two kind of response varies with the manufacturing stage, as evidenced in sect. 3. For each stage, the validation of the FE model in terms of single vibration modes can be carried out up to this transition frequency at most. Although experimental modal analysis allowed identifying modes up to 400 to 450 Hz, for the sake of brevity the numerical–experimental comparison reported in Tab. 2 is limited to the first 20 experimental modes of each manufacturing stage.

However, together with mode pairing it is interesting to verify if the model is capable of reproducing the soundboard dynamic response over a wider frequency range. To this end the FE model was used for calculating the FRF up to 4 kHz. Fig. 10 shows the comparison between calculated and experimental mobility: the soundboard is excited in the same position considered in Fig. 4 (i.e. close to the bridge, in correspondence with the crossing of the $A\sharp_4$ string) and the output vibration is measured three ribs apart, towards the back of the piano. In the numerical calculations the damping data are those obtained from modal testing, where available, while the non-dimensional damping ratio was set to 2 % for all modes at higher frequency.

Looking at Fig. 10, it is the authors' opinion that the poor match below 100 Hz is probably due to the fact that the FE model does not include the rim, i. e. the soundboard support is assumed to be infinitely rigid. Therefore the modes resulting from the coupling with the supporting structure cannot be reproduced by the numerical simulation. At higher frequency the effect of the boundary conditions becomes less and less important and the agreement between calculated and measured mobility is in general satisfactory, although some shift in the position of resonances and anti-resonances can be observed.

7. Conclusions

The results obtained from a comprehensive modal analysis campaign were used to validate and update the finite element model of a grand piano soundboard. Considering the characteristics of the soundboard structure and of its manufacturing process, it was decided to develop the finite element model of a structure with increasing complexity, by following the same progressive stages adopted in the instrument construction. Therefore, testing and simulation proceeded in parallel, so as to improve the model capability of capturing the dynamic behaviour of the real structure, which depends on the combination of many parameters, ranging from material properties to geometric configuration, from process-induced stresses to boundary conditions.

Bearing in mind the unavoidable uncertainties which are typical of a complex natural material like wood, at STAGE 1 the soundboard material properties were updated so as to minimise the difference between calculated and experimental vibration modes, in terms of both natural frequencies and mode shapes. Any other model feature was left unvaried. Then the FE simulation of the manufacturing process proceeded in STAGE 2, 3 and 4, without any further tuning of the material properties and, at each stage, the agreement between numerical results and experimental data was verified.

Experimental modal analysis allowed identifying the vibration modes only in the low-frequency range, where the soundboard dynamic response is dominated by individual modal resonances. In the specific case of the tested piano soundboard, this corresponds to approximately 400 to 450 Hz maximum. Accordingly, model validation in terms of numerical–experimental comparison of single natural frequencies and corresponding mode shapes could be performed only in this frequency range. The number of experimental modes which are involved in this validation process ranges from 34 to 52, depending on the manufacturing stage. Once that the FE model was properly tuned in terms of individual vibration modes, numerical and experimental FRF's were compared, to verify the model capability of reproducing the structure's dynamic behaviour also in the mid/high-frequency

range, which is characterised by increasing modal density and coupled multi-mode response.

The results obtained are encouraging and the FE model that has been set up can be considered the first fundamental step towards the development of a vibroacoustic model of the piano soundboard. The main advantage of the modelling approach proposed in this paper is that it can provide a better understanding of the effect of the manufacturing process and of specific design solutions on the soundboard vibration properties and on its consequent acoustic performance.

The research activity is going on and the authors are developing an upgraded version of the FE model which includes the soundboard supporting structure. This is expected to solve the problem of the systematically overestimated natural frequencies in STAGE 3, and of the missing effects of the coupling between the soundboard and the rim, thus overcoming the limits of the simplifying assumption of infinitely rigid supporting structure (clamped boundary). A boundary element model is being developed in parallel, which will be used to predict the sound field radiated from the piano soundboard on the basis of the FE model output. The final objective of this vibroacoustic predictive tool will be that of providing support to the entire design process of a new musical instrument.

References

[1] P. H. Bilhuber, C. A. Johnson, The Influence of the Soundboard on Piano Tone Quality, The Journal of the Acoustical Society of America 11 (3) (1940) 311–320. doi:10.1121/1.1916039.

[2] H. Suzuki, Vibration and sound radiation of a piano soundboard, The Journal of the Acoustical Society of America 80 (6) (1986) 1573–1582. doi:10.1121/1.394321.

[3] J. Kindel, I.-C. Wang, Modal Analysis and finite element analysis of a piano soundboard, in: 5th International Modal Analysis Conference (IMAC), 1987, pp. 1545–1549.

[4] H. A. Conklin, Design and tone in the mechanoacoustic piano. Part II. Piano structure, The Journal of the Acoustical Society of America 100 (2) (1996) 695–708. doi:10.1121/1.416233.

[5] N. Giordano, A. J. Korty, Motion of a piano string: Longitudinal vibrations and the role of the bridge, The Journal of the Acoustical Society of America 100 (6) (1996) 3899–3908. doi:10.1121/1.417219.

[6] N. Giordano, Simple model of a piano soundboard, The Journal of the Acoustical Society of America 102 (2) (1997) 1159–1168. doi:10.1121/1.419868.

[7] N. Giordano, Sound production by a vibrating piano soundboard: Experiment, The Journal of the Acoustical Society of America 104 (3) (1998) 1648–1653. doi:10.1121/1.424377.

[8] N. Giordano, Mechanical impedance of a piano soundboard, The Journal of the Acoustical Society of America 103 (4) (1998) 2128–2133. doi:10.1121/1.421358.

[9] N. Giordano, M. Jiang, Physical modeling of the piano, EURASIP Journal on Applied Signal Processing 2004 (7) (2004) 926–933. doi:10.1155/S111086570440105X.

[10] J. Chabassier, A. Chaigne, P. Joly, Modeling and simulation of a grand piano, The Journal of the Acoustical Society of America 134 (1) (2013) 648–665. doi:10.1121/1.4809649.

[11] J. Berthaut, M. N. Ichchou, L. Jézéquel, Piano soundboard: structural behavior, numerical and experimental study in the modal range, Applied Acoustics 64 (11) (2003) 1113–1136. doi:10.1016/S0003-682X(03)00065-3.

[12] T. R. Moore, S. A. Zietlow, Interferometric studies of a piano soundboard, The Journal of the Acoustical Society of America 119 (3) (2006) 1783–1793. doi:10.1121/1.2164989.

[13] A. Mamou-Mani, J. Frelat, C. Besnainou, Numerical simulation of a piano soundboard under downbearing, The Journal of the Acoustical Society of America 123 (4) (2008) 2401–2406. doi:10.1121/1.2836787.

[14] A. Mamou-Mani, S. Le Moyne, F. Ollivier, C. Besnainou, J. Frelat, Prestress effects on the eigenfrequencies of the soundboards: Experimental results on a simplified string instrument, The Journal of the Acoustical Society of America 131 (1) (2012) 872–877. doi:10.1121/1.3651232.

[15] A. Chaigne, B. Cotté, R. Viggiano, Dynamical properties of piano soundboards, The Journal of the Acoustical Society of America 133 (4) (2013) 2456–2466. doi:10.1121/1.4794387.

[16] K. Fenner, Resonanzboden in Neubau und Reparatur, EuroPiano (1) (1998) 14+.

[17] D. J. Ewins, Modal testing : theory, practice, and application, Research Studies Press, 2000.

[18] J. S. Bendat, A. G. Piersol, Random data : analysis and measurement procedures, Wiley, 2000.

[19] W. Heylen, S. Lammens, P. Sas, Modal analysis theory and testing, Katholieke Universiteit Leuven, Faculty of Engineering, Dept. of Mechanical Engineering, Division of Production Engineering, Machine Design and Automation, 1998.

[20] N. M. Maia, J. M. Montalvão e Silva, Theoretical and experimental modal analysis, Research Studies Press, 1997.

[21] H. Van der Auweraer, P. Guillaume, P. Verboven, S. Vanlanduit, Application of a Fast-Stabilizing Frequency Domain Parameter Estimation Method, Journal of Dynamic Systems, Measurement, and Control 123 (4) (2001) 651–658. doi:10.1115/1.1410369.

[22] K. Ege, X. Boutillon, B. David, High-resolution modal analysis, Journal of Sound and Vibration 325 (4-5) (2009) 852–869. doi:10.1016/j.jsv.2009.04.019.

[23] Abaqus User Manual (2010).

[24] V. Bucur, Acoustics of wood, Springer, 2006.

[25] O. C. Zienkiewicz, R. L. Taylor, The Finite Element Method, Vol. 2: Solid Mechanics, Butterworth Heineman, 2000.

[26] R. J. Allemang, D. L. Brown, Correlation coefficient for modal vector analysis, in: Proceedings of the International Modal Analysis Conference & Exhibit, 1982, pp. 110–116.

A. Naming convention for orthotropic elastic constants

The engineering constants E_i, ν_{ij}, G_{ij} reported in Tab. 1 are defined in terms of elastic compliance as follows:

$$\begin{Bmatrix} \varepsilon_1 \\ \varepsilon_2 \\ \varepsilon_3 \\ \gamma_{23} \\ \gamma_{31} \\ \gamma_{12} \end{Bmatrix} = \begin{bmatrix} 1/E_1 & -\nu_{21}/E_2 & -\nu_{31}/E_3 & 0 & 0 & 0 \\ -\nu_{12}/E_1 & 1/E_2 & -\nu_{32}/E_3 & 0 & 0 & 0 \\ -\nu_{13}/E_1 & -\nu_{23}/E_2 & 1/E_3 & 0 & 0 & 0 \\ 0 & 0 & 0 & 1/G_{23} & 0 & 0 \\ 0 & 0 & 0 & 0 & 1/G_{31} & 0 \\ 0 & 0 & 0 & 0 & 0 & 1/G_{12} \end{bmatrix} \begin{Bmatrix} \sigma_1 \\ \sigma_2 \\ \sigma_3 \\ \tau_{23} \\ \tau_{31} \\ \tau_{12} \end{Bmatrix}, \quad \text{(A.1)}$$

with

$$-\nu_{21}/E_2 = -\nu_{12}/E_1, \qquad -\nu_{31}/E_3 = -\nu_{13}/E_1, \qquad -\nu_{32}/E_3 = -\nu_{23}/E_2,$$

for a total of 9 independent elastic constants. The elasticity axes (1, 2, 3) are aligned to the anatomical directions (L, R, T), i. e. longitudinal, radial, and tangential to the annual rings.

List of acronyms

CAD	Computer Aided Design
CNC	Computer Numerical Control
DSA	Design Sensitivity Analysis
FE (FEM)	Finite Element (Method)
FFT	Fast Fourier Transform
FRF	Frequency Response Function
IRF	Impulse Response Function
LSCE	Least Squares Complex Exponential
MAC	Modal Assurance Criterion

List of Figures

List of Tables

Contents